TÜBİTAK

Turk J Elec Eng & Comp Sci, Vol.20, No.6, 2012, © TÜBİTAK
doi:10.3906/elk-1101-1024

Optimal in vitro realization of pulsatile coronary artery flow waveforms using closed-loop feedback algorithms with multiple flow control devices

Serdar YILMAZ[1,*], **Onur TOKER**[1], **Nurullah ARSLAN**[2], **Herman SEDEF**[3]
[1] *Department of Electrical and Electronics Engineering, Fatih University, İstanbul-TURKEY*
e-mails: {syilmaz, onur}@fatih.edu.tr
[2] *Department of Genetics and Bioengineering, Fatih University, İstanbul-TURKEY*
e-mail: narslan@fatih.edu.tr
[3] *Department of Electronics and Communications Engineering, Yıldız Technical University, İstanbul-TURKEY*
e-mail: sedef@yildiz.edu.tr

Received: 14.01.2011

Abstract

In this paper, we study optimal in vitro realization of pulsatile coronary artery flows using newly proposed closed-loop feedback algorithms with a clearly defined mathematical performance objective, and we compare several flow control device technologies in terms of their ability to generate pulsatile flow signals as accurately as possible. In the literature, there are several published results for in vitro pulsatile flow realization systems. However, most of the proposed systems operate in an open-loop setting and use a single flow control device, and their performance is assessed mostly by graphical means without a clearly defined mathematical performance objective. Furthermore, some authors take the average of the generated pulsatile flow and compare it with the desired flow signal for performance analysis. What makes this work different from other published results in this area are: 1) the use of closed-loop feedback control rather than an open-loop approach; 2) the use of a clearly defined mathematical performance objective rather than a visual comparison of the generated and desired flow graphs; 3) newly proposed control algorithms with demonstrated performance improvements as compared to the published ones; 4) the use of multiple flow control devices, their performance comparisons, and optimal technology selection; and 5) not taking the average of the generated flow signal over several cycles for performance assessment, but instead using the nonaveraged actual flow signal and comparing it with the desired one. In pulsatile flow realization, what is important is the L_1 distance between the desired and delayed versions of the generated flows in the steady state regime, and the defined mathematical performance objective is completely based on this point. Furthermore, there are 3 different flow control devices that are comparatively analyzed: the pneumatic valve, the servo valve, and an AC inverter driving a centrifugal pump. Finally, there are several new closed-loop control algorithms proposed in this paper: P-Σ, P-Σ predictive, P-Σ look ahead, and model-based nonlinear feed-forward, feed-forward predictive, and feed-forward look-ahead control. Each algorithm's performance is compared with that of PID performance as a benchmark test to

*Corresponding author: Department of Electrical and Electronics Engineering, Fatih University, İstanbul-TURKEY

demonstrate performance improvements. By proper selection of the flow control device, and optimal selection of the control algorithm and its parameters, we were able to achieve up to 75% reduction in error.

Key Words: *Pulsatile waveforms, coronary artery, feedback control, in vitro realization*

1. Introduction

Cardiovascular diseases are among the most important causes of physical disabilities and deaths in the western world [1]. Moreover, cardiovascular diseases are also suspected to be the major cause of a significant percentage of deaths in developing countries [2]. The function of the cardiovascular system is to transport blood to all tissues and organs. The flexibility and the geometry of the arteries, as well as the blood viscosity, are known to affect the blood flow velocity [3,4]. Measurements of arterial blood flow velocity profiles can be used to detect abnormal conditions in the cardiovascular system. Indeed, variable blood pressure and abnormalities in flow rates gradually affect the whole body including cells, biochemical signals, tissues, and organs [5-8]. Problems like artificial hearts, artificial organs, graft design, hemodialysis-related studies, and rheology can greatly benefit from blood flow-related research [1].

The main motivation in this paper is to develop new ideas and improved techniques that will enable accurate in vitro realization of blood flow waveforms in the laboratory environment. Analysis of flow profiles in different cross sections, and the use of these experimental measurements, is expected to result in better designs. As an example, consider the graft design problem. A proposed design can be analyzed with respect to turbulence and other effects by generating certain blood flow patterns on test equipment. More precisely, before it is implanted into a patient, it can be carefully optimized by experimental measurements and repeated in vitro tests. Therefore, accurate in vitro realization of blood flow patterns is of extreme importance. In this paper, we study the optimal in vitro realization of blood flow patterns using new closed-loop control algorithms, define a mathematical performance objective to accurately assess performance of different algorithms, and, finally, comparatively evaluate different flow control device technologies.

There are several published papers in the literature on blood flow and its effects on the cardiovascular system. Part of these papers, which can be classified as numerical or simulation-based, basically concentrate on the mathematical modeling of fluid flow and the geometric data of the blood vessel [9-12]. A fundamental problem in this numerical approach is that the simulation duration is increased by reducing the simulation time step size, or by reducing the spatial dimensions of the cells used in finite element modeling. Depending on the time step size, the dimensions of the cells, and the complexity of the model, it may take from a few minutes to several hours, or even more, to obtain simulation results. Nevertheless, simulation results do not reflect the actual system with full accuracy because the simulated mathematical models do not include all of the dynamics and parameters of the actual system. Research efforts based on experimental measurements conducted in laboratory environments do not suffer from such drawbacks; they provide more accurate results and hence will result in better designs compared to the ones based on simulation studies. However, experimental measurements may require a bigger investment in lab equipment, may require more skilled staff to operate the system, and, in general, may be more difficult to manage compared to a pure simulation-based research environment. In general, experimental and numeric/simulation based studies have their own advantages/disadvantages, and both approaches are widely used in the literature. In this paper, we adopt the experimental approach rather than a numeric/simulation-based one.

Rapid developments in magnetic resonance imaging (MRI) techniques have enabled various noninvasive

measurements, in particular blood flow measurements in various parts of the human body. Because of the availability of such data, in vitro studies have become quite popular [13]. Although blood flow rates in arteries can be measured by noninvasive methods as well, long-term in vivo studies on real patients are not practical [13] and might even involve certain health risks for the patient. Therefore, most researchers have adopted a hybrid approach; first, noninvasive methods are used to measure blood flow rates from real patients, and, following that, all of the subsequent research and all analysis/design are conducted on test systems via experimental means [4].

There are several experimental systems reported in the literature for in vitro studies. These systems include flow control devices, flow measurement devices, a graft model, a suitable fluid, and tubing structures [1,9-26]. The test system is generally a scaled-up version of the actual graft system. There are certain fixed ratios between their geometries, which are defined by the Reynolds [1,9,11-21] and Womersley [1,13-15,17,20,21] numbers. According to this scaling theory, which is known as dynamic similarity, viscosity, flow rate, and periods are recalculated for the test system based on actual in vivo data. More precisely, the Reynolds number is defined as:

$$Re = \frac{\rho V D}{\mu}, \tag{1}$$

where V is the mean fluid velocity, D is the diameter of the pipe, μ is the dynamic viscosity, and $\rho$is the density of the fluid. The Womersley number is defined as:

$$\alpha = R\left(\frac{\omega\rho}{\mu}\right)^{1/2}, \tag{2}$$

where R is the radius of the pipe, ω is the angular frequency of the oscillations, and ρ and μ are the density and the dynamic viscosity of the fluid, respectively. The dynamic similarity theory basically says that if 2 pulsatile flow systems are related to each other by pure geometric, frequency, velocity, and viscosity scaling factors, their behaviors are similar as long as this scaling preserves the Reynolds and Womersley numbers. Generally, a glycerin-water mixture is used as test fluid and the proportions are adjusted so that its index of refraction matches that of the material of the graft model. As for the graft model, both elastic rubber such as flexible silicon based materials [1,15,22,24] and inflexible materials such as Plexiglas [11-14,16,17,21] are commonly used. Fluid flow rates can be measured by a magnetic flow velocity meter [12-14,17,19-21,23], an ultrasonic flow meter, a photomultiplier [1], laser Doppler anemometry (LDA) [11,12,15,16,18,19,21], particle image velocimetry (PIV) [1,13,14,20], or by charge-coupled device (CCD) cameras. While magnetic and ultrasonic flow meters give the global flow rate of the model, LDA and PIV can be used for local flow velocity measurements, and CCD cameras can be used for flow visualization. There are also several different technologies for flow control. These include injection pumps [16], piston pumps [13-15,17,26], centrifugal pumps [1,9-12,18-25], gear pumps [26], and other types of pumps and valves [1,9-12,14-26]. Several research teams have used a constant speed motor pump and generated a pulsatile flow by manipulating a valve [1,9-12,16,18-25]. Another group of researchers used piston pumps to generated pulsatile flows [13-15,17,26]. In this paper, we comparatively evaluate the following flow control devices: a pneumatic valve, a servo valve, and an AC inverter driving a centrifugal pump.

To the best of the authors' knowledge, in all of these published research papers, there was no clear mathematical performance criteria used to assess the performance of the system, or for comparison with other systems. Most of the analysis was done by pure graphical means, and in certain cases, generated pulsatile blood flow was first averaged over 15 cycles and then compared with the desired blood flow rate, again by

using pure graphical means only [26]. Furthermore, a significant portion of researchers use only open-loop techniques to generate a pulsatile flow pattern. A sinusoidal or sinusoidal-like input is given to the open-loop system, and a pulsatile flow, usually of a different shape, is generated on the experimental system [13,14,17]. The initial input to the open-loop system is then adjusted systematically by a trial and error procedure so that the generated pulsatile flow matches the desired flow. This approach has a number of disadvantages. First, the input signal synthesized by a trial and error procedure will most likely result in a nonperfect match. Second, due to unmodeled dynamics, the time-varying nature of systems, and error build-up, the generated pulsatile flow may be quite different in each cycle. Finally, and worst of all, the system will have no built-in mechanism to eliminate or reduce such discrepancies. The authors were able to find only one paper published in the literature utilizing closed-loop (proportional integral [PI]) control techniques [10]. This system was built with a constant speed pump and proportional valve, but no mathematical performance criteria were defined, and performance was assessed only by graphical means. In 2010, Tsai and Savaş [26] reported a flow control system to simulate various blood flow signals in the human body, but they also carried out all of the experiments in an open-loop control setting. Their experimental system included a piston pump, a gear pump, a back pressure valve, 2 motors of 600 W and 400 W, and a computer system with a data acquisition card.

This paper is organized as follows: in Section 2 we present the materials and methods; in Section 3 we discuss modeling, repeatability, nonlinearity, and hysteresis issues; in Section 4 we define a mathematical performance objective; in Section 5 we present proportional integral derivative (PID) controller performance data for benchmark tests; in Section 6 we propose new closed-loop feedback algorithms and evaluate their performance; and, finally, in Section 7 some concluding remarks are made.

1.1. Abbreviations

AC	Alternating current	OTA	Output triangular amplitude
BOP	Basic operator panel	PC	Personal computer
CCD	Charge-coupled device	PI	Proportional integral
DAQ	Data acquisition	PID	Proportional integral derivative
DC	Direct current	PIV	Particle image velocimetry
HE	Hysteresis magnitude	PVC	Polyvinyl chloride
HIL	Hardware in the loop	PWM	Pulse width modulation
LDA	Laser Doppler anemometry	P-Σ	Proportional rate-limited sum
MD	Maximum difference	VFD	Variable frequency drive
MRI	Magnetic resonance imaging	*rLim*	Rate limiter function

2. Materials and methods

The schematic of the experimental system used in this study is shown in Figure 1. At the center of the whole system there is a personal computer (PC) equipped with a data acquisition (DAQ) card. There are 2 flow measurement devices, which are Siemens magnetic flow meters, and 3 flow control devices, which are a centrifugal pump driven by a Siemens inverter, a Bürkert solenoid valve, and an Ecoflo pneumatic valve. Different artificial graft models made from Plexiglas or similar transparent material can be tested against different pulsatile flow patterns. For local flow velocity measurements, the system has a laser Doppler anemometry (LDA) device and a line laser that can be used with a camera for flow visualization studies. These 2 pieces of equipment are not shown in Figure 1 because the emphasis of this paper is not on a particular graft design and the associated measurements; it is rather about generating different pulsatile flow waveforms as accurately as possible using

newly proposed closed-loop control techniques and different flow control devices. In a subsequent paper, the authors are planning to test different graft designs against various pulsatile flow patterns that are generated using the test equipment described above, together with the closed-loop control techniques developed in this study.

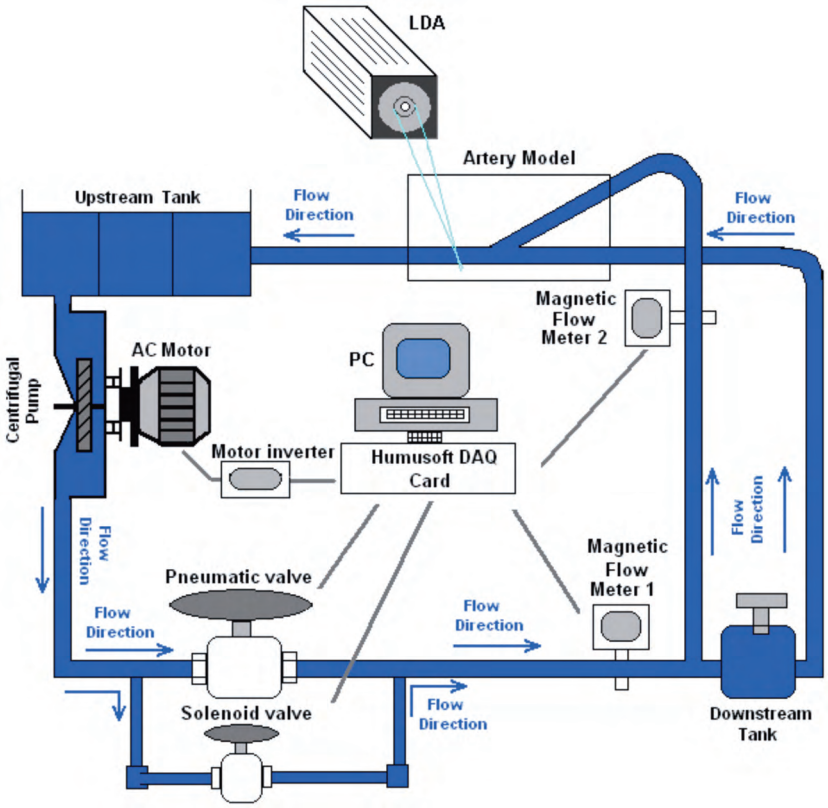

Figure 1. System block diagram.

The test system basically has 5 different main components: flow control devices, a data acquisition and processing unit (DAQ card and PC), measurement devices, a graft model, and a complex network of tanks and pipes. In the following subsections, each component is discussed in detail.

2.1. Flow control devices

In the test system, there is a proportional pneumatic valve, Ecoflo-GV, with an electropneumatic positioner, YT-1000L. The second flow control device is a proportional solenoid valve from Bürkert, type 2835. The third flow control device is a centrifugal pump (Type U83B1, Fasco), driven by a Siemens SINAMICS G110 inverter. The proportional pneumatic valve has a standard current input of 4-20 mA, which is driven by the DAQ card, followed by a simple but industrial grade voltage-to-current (V/I) converter. The proportional solenoid valve has a Bürkert 8605 controller, which basically converts the input voltage of 0-10 V to a pulse width modulation (PWM) signal driving the solenoid coil and hence controlling the valve. The DAQ card drives the Bürkert 8605 controller directly from one of its analog outputs of 0-10 V. The SINAMICS G110 inverter is a variable-frequency drive (VFD) equipped with a BOP (basic operator panel) that enables the selection of various drive parameters and input type selection. In this test system, the SINAMICS G110 inverter is configured to work with voltage

input of 0-10 V, which is driven directly by the analog output of the DAQ card. The inverter generates an AC signal with a frequency proportional to the input. By changing the frequency of the AC signal, it is possible to control the motor speed and hence to have flow control at the centrifugal pump.

2.2. Data acquisition and processing unit

The data acquisition and processing unit is basically a PC with a Humusoft MF614 DAQ card. The PC has MATLAB/Simulink, and all of the experiments are done using the hardware in the loop (HIL) technique, which enables rapid prototyping and performance analysis. In the subsequent sections, newly proposed control algorithms will be discussed in detail. The Humusoft DAQ card has 8 analog inputs and 4 analog outputs. It also has 8 digital inputs, 8 digital outputs, and a timer, but these features are not used in this test system. The Humusoft DAQ card drives flow control devices via its analog outputs and gets flow rates from measurement devices via its analog inputs. Because of the real-time HIL simulation, where the actual controlled hardware is used in the control loop instead of its mathematical model, all of the experiments are done as easily as if one is conducting a pure computer simulation study, but indeed actual experiments are conducted with real measurements. Throughout the paper, all of the closed-loop control experiments are conducted with a 100-Hz sampling rate.

2.3. Measurement devices

There are 2 Siemens MAG 5000 magnetic flow meters used in the test system. The MAG 5000 magnetic flow meter provides high precision measurements with an error rate as low as 0.5%. The desired output format can be configured as digital or analog via the flow meter's user control panel. The flow meter in this study is configured to output a voltage of 0-10 V. By using the control panel, it is also possible to assign a nonzero minimum flow rate to the 0-V voltage level and a maximum flow rate to the 10-V voltage level. This enables higher resolution measurements for the overall system, because the flow meter's output is directly connected to the DAQ card's analog input of 0-10 V. The main fluid flow on the experimental system is divided into 2 substreams for an artery bypass implant application. To measure the flow rates of both substreams, 2 different magnetic flow meters are utilized.

2.4. Coronary in vitro bypass model

Artificial grafts used in this study are manufactured from transparent Plexiglas tubes. For laser Doppler measurements or flow visualization studies, the whole bypass model must be placed inside a rectangular box filled with a water-glycerin mixture, with an index of refraction equal to the index of refraction of the Plexiglas used in the test system. The rectangular box enables perfectly perpendicular entry of the laser beam used in LDA or the line laser used in flow visualization measurements.

2.5. Network of pipes and tanks

In Figure 1, the direction of the fluid flow is shown by arrows labeled "Flow direction". There are 2 tanks in the system, the upstream and downstream tanks. The upstream tank is the tank in which most of the fluid is stored. The centrifugal pump takes the fluid from this tank and then pumps it into the system. The downstream tank is the other tank in the system, and it is installed to eliminate the effects of turbulence and bubbles before fluid entry into the artificial coronary bypass model. There is also a long straight pipe after the flow control valves.

The main reason for this is again to eliminate the effects of turbulence and other irregularities in the flow before the magnetic flow meters. The liquid used in the system is a mixture of 60% glycerin and 40% water. There is a check valve installed at the top of the downstream tank and a manometer just after the pump. The maximum observed fluid pressure is about 2 bars. A significant portion of the whole pipe network is constructed from pressure-resistant PVC pipes.

3. Preliminary identification tests on flow control devices

In order to build a high performance closed-loop control system, it is essential to know the limitations, nonlinearities, hysteresis, and repeatability problems of the actuator devices. In this section we conduct the following tests for the flow control devices: 1) repeatability test, 2) hysteresis test, and 3) nonlinearity test. These preliminary identification tests will provide an indication of which device and closed-loop control algorithm is more likely to perform better, and will give extremely valuable insight about the operation of the whole system. In all of these tests, various test inputs are applied to the open-loop system and the system response is recorded for further analysis. In all of the tests discussed in this section, while the centrifugal pump is being tested, all of the valves are kept at a constant position (either both fully open, or one of them closed and the other one open), whereas when one of the valves is under a particular test, the other valve is kept at a full blocking position and the centrifugal pump speed is kept at a constant speed.

3.1. Repeatability tests of flow control devices

Control equipment may exhibit either small or large time-varying behaviors. In other words, in each experiment, one may observe either slight or major differences in the device characteristics. This makes the control problem difficult, especially if the differences are major. In this subsection, we analyze all 3 flow control devices in terms of their repeatability characteristics. The test signal used basically consists of pseudorandom steps of 5 to 10 s in duration, with "randomly" selected levels in the range of 0-10 V. Indeed, this range is divided into several small subintervals, and each time, one of these levels is chosen in a pseudorandom fashion. Different DC input levels will be applied to these flow control devices for 5 to 10 s, basically to allow the device to reach a steady state, and the device response will be recorded. Each DC input level will be applied to the system a couple of times, and both the minimum and maximum observed response will be plotted versus the applied input level. If there is a major difference between the minimum and maximum response graphs, one can conclude that the system has a major repeatability problem. On the other hand, if these 2 graphs overlap and there is a significant match, then the system can be classified as repeatable.

3.1.1. Centrifugal pump repeatability test

The centrifugal pump used in the test system is driven by the AC inverter, which in turn is controlled by the DAQ card's analog voltage output. For reasons of safety and equipment protection, the maximum DAQ analog voltage output is limited to 9 V. It has been observed that the pump is able to increase the flow rate from 100 mL/s to 900 mL/s, within 10 s. Therefore, each pseudorandomly generated DC voltage is applied to the AC inverter for 10 s, which is expected to give enough time for the test system to respond and reach another steady flow rate state.

For the repeatability experiment, the input voltage range of 0-9 V is divided into 46 subintervals of 0.2 V in length, and for each such subinterval, a DC signal is generated for 10 s. Each DC level is generated 5

different times, which are selected using a pseudorandom generator. The total experiment duration is 2350 s.

Figure 2 shows the results of the repeatability test for the centrifugal pump. The blue curve is the maximum observed steady state response, and the red curve is the minimum observed steady state response. First of all, since the 2 curves are very close to each other, the centrifugal pump can be classified as a repeatable system. We also see that for the input voltage range of 0-1 V, there is almost no induced flow, and after that voltage range there is a linear-like relationship between the applied voltage and the generated flow. However, after a flow rate range of 800-850 mL/s, the linear-like relationship is lost.

3.1.2. Pneumatic valve repeatability test

The pneumatic valve in the test system is driven by the electropneumatic positioner, which is directly connected to the DAQ card's analog voltage output. The maximum DAQ analog voltage output is 10 V. It has been observed that even in the worst case, i.e. even for large movements, the pneumatic valve is able to respond and reach a steady state after 5 s. Therefore, the step duration is selected as 5 s. The input voltage range of 0-10 V is divided into 34 subintervals and each DC level is applied 10 different times at various time instants. The total experiment duration is 1750 s.

The result of the repeatability test for the pneumatic valve is shown in Figure 3. As in the previous repeatability test, the blue curve is the maximum observed steady state response and the red curve is the minimum observed steady state response. First of all, nonlinearity in the behavior is much more significant and the repeatability is worse than in the case reported in Figure 2. Furthermore, for input signals in the interval of 1.5-2.5 V, the flow rate is rather flat. Before this interval, the flow versus applied voltage behavior is linear-like, but after this interval, it is significantly nonlinear.

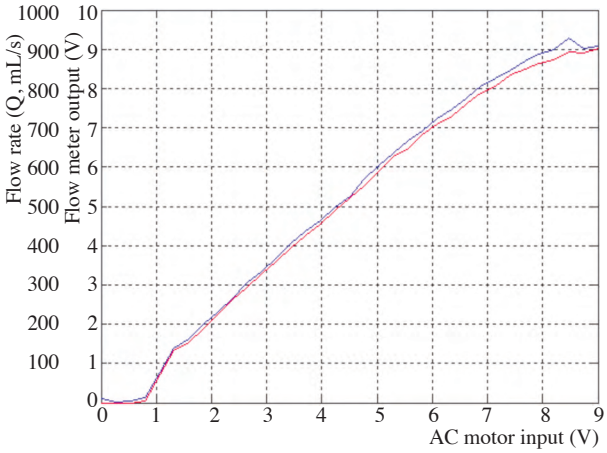

Figure 2. Centrifugal pump repeatability experiment results.

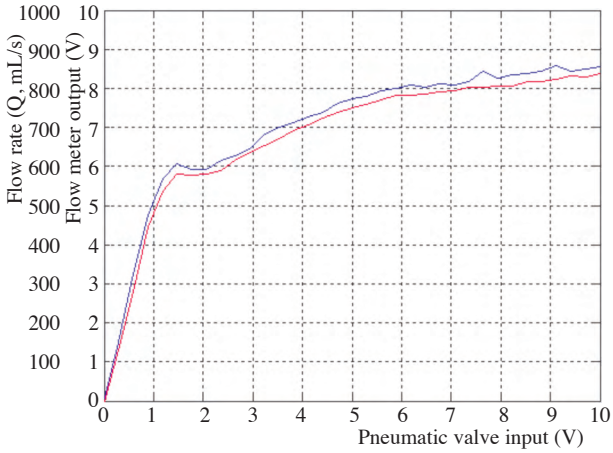

Figure 3. Pneumatic valve repeatability experiment duration.

3.1.3. Solenoid valve repeatability test

The solenoid valve in the test system is driven by a DC-to-PWM converter controlling the solenoid coil. The DC input of the converter is connected to the DAQ analog voltage output. It has been observed that the response of the solenoid valve is faster; however, we have again chosen the step duration of 5 s for this experiment. The interval of 0-10 V is divided into 20 equal subintervals and each DC level is repeated 10 different times. The total experiment duration is 1050 s.

The result of the repeatability test for the solenoid valve is shown in Figure 4. In terms of repeatability, it is not as good as the centrifugal pump; however, the device exhibits an almost linear relationship between the flow rate and the applied input voltage.

3.2. Hysteresis behavior of flow control devices

In this section, we study the hysteresis behavior of the flow control devices used in the test system. For each flow control device, a triangular wave is applied for a period of 100 s in an open-loop setting and the system response (flow rate) is recorded. To assess the "magnitude" of the hysteresis (HE), one can compute the maximum difference (MD) between the "loading" (upper curve) and "unloading" (lower curve) flow rate versus applied input voltage curves (see Figure 5). If the output triangular wave amplitude is denoted by the output triangular amplitude (OTA), the HE can be computed as:

$$HE = \frac{MD}{OTA}100. \tag{3}$$

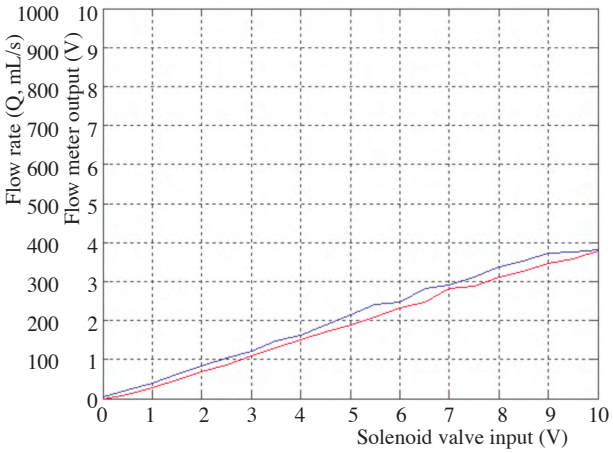

Figure 4. Solenoid valve repeatability test results.

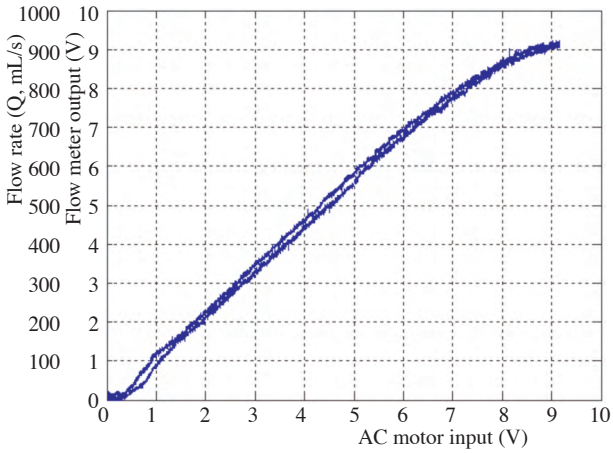

Figure 5. Centrifugal pump hysteresis graph.

3.2.1. Centrifugal pump hysteresis

In this test, a triangular wave with a peak-to-peak amplitude of 9 V is applied for a period of 100 s to the input of the AC motor inverter, which drives the centrifugal pump. The test is conducted in an open-loop setting and the result is shown in Figure 5.

Similar to the repeatability test graph shown in Figure 2, the centrifugal pump exhibits nonlinear behavior for flow rates below 100 mL/s and above 800-850 mL/s. However, based on the experimental data of the HE, it is computed as 3%, which indicates that there is almost no hysteresis behavior in the centrifugal pump system.

3.2.2. Pneumatic valve hysteresis

For the pneumatic valve hysteresis analysis experiment, the centrifugal pump is driven at a constant speed, and a triangular wave with a peak-to-peak amplitude of 2.5 V is applied to the pneumatic valve electropneumatic positioned input. The result of this open-loop test is shown in Figure 6.

Especially in the input voltage range of 0.3-1.3 V, which roughly corresponds to a flow rate region of 50-550 mL/s, significant hysteresis behavior is clearly visible. The HE is computed as 18%, which is high enough to make its closed-loop control a difficult task.

3.2.3. Solenoid valve hysteresis

The solenoid valve hysteresis test is done by applying a triangular wave with a peak-to-peak amplitude of 6 V for a period of 100 s to its controller apparatus input. During the test, the centrifugal pump is kept at a constant speed and the pneumatic valve is kept at a constant blocking position. The test is again conducted in an open-loop setting and the results are shown in Figure 7.

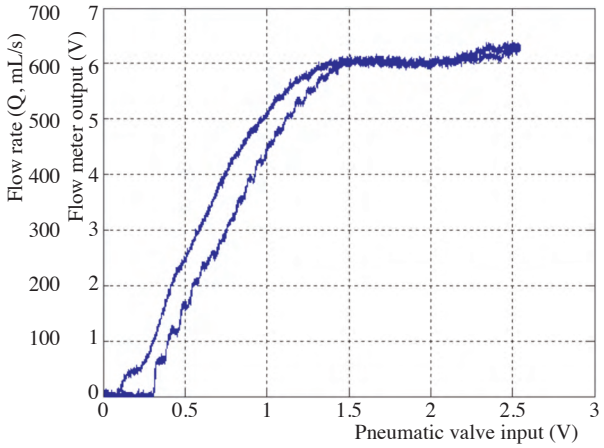

Figure 6. Pneumatic valve hysteresis graph.

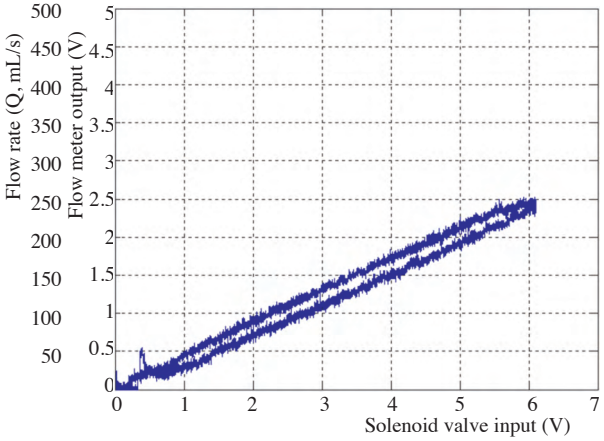

Figure 7. Solenoid valve hysteresis graph.

The HE is calculated as 8%, which can be classified as "mild" hysteresis when compared with that of the pneumatic valve (18%) and the centrifugal pump (3%).

3.3. Nonlinear model development

In this section, we consider static nonlinear modeling of the flow control devices. If repeatability and hysteresis problems are ignored, and if the flow control device's internal dynamics are ignored as well, a static nonlinear model may be used to linearize the device. A static nonlinear model can be used in the linearization of the flow control device and can hence simplify the closed-loop control design procedure. More precisely, the controller design can be done for a "fictitious" linear plant, and then the inverse of the static nonlinear map may be augmented to the designed controller.

In the future, the authors do plan to do dynamic nonlinear modeling. More specifically, the authors plan to consider Hammerstein models and to design closed-loop controllers based on these models. However, in this study, flow control device internal dynamics are not modeled. Therefore, in all of the tests given below, after a particular DC input is applied, the steady state flow rate is considered as the "response" or "output" of the nonlinear system.

3.3.1. Centrifugal pump nonlinear model development

In this modeling experiment, more than 50 different DC values are applied as input and the steady state flow rates are recoded. During this experiment, the pneumatic valve was fully open.

For nonlinear modeling, we first choose the order of the polynomial, and then use the least squares method to find the optimal L_2 approximation. For the centrifugal pump, the following third-order approximation:

$$p(x) = -0.010989x^3 + 0.1049x^2 + 0.98425x - 0.26017, \tag{4}$$

resulted in a good match for the input-output behavior shown in Figure 8.

3.3.2. Pneumatic valve nonlinear model development

In this subsection, we investigate the modeling of the pneumatic valve.

During the identification tests, the solenoid valve was fully closed and the AC motor was driven at a constant speed by an 8-V input signal. The pneumatic valve showed quite nonlinear behavior in the vicinity of flow rates of 600 mL/s, which corresponds to the input voltage range of 1-2.5 V. More samples are taken in this region, where the input-output behavior changed from a linear-like trend to another one. Difficulty of the flow control around flow rates of 600 mL/s was expected theoretically and was really experienced, as well, during the various tests done for this study. The following seventh order polynomial:

$$p(x) = 0.00024x^7 - 0.00915x^6 + 0.13904x^5 - 1.0843x^4 + 4.5946x^3 - 10.357x^2 + 11.818x + 0.6572, \tag{5}$$

is obtained as an approximate nonlinear model for the input-output behavior shown in Figure 9. Again, the optimal L_2 approximation techniques are used for model development.

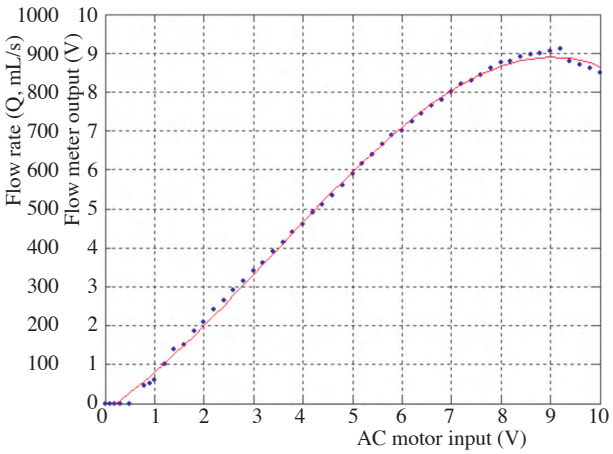

Figure 8. Centrifugal pump input-output graph.

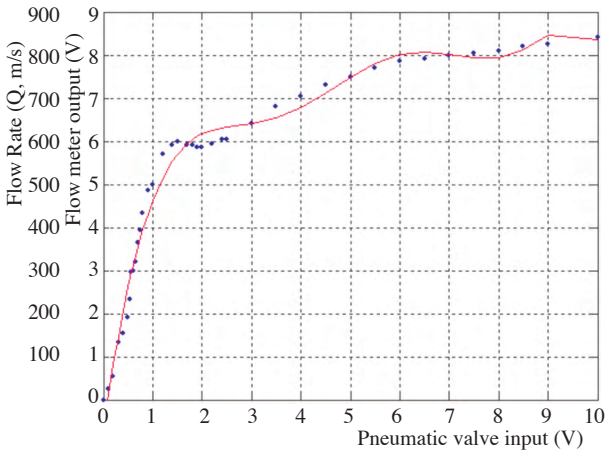

Figure 9. Pneumatic valve input-output graph.

3.3.3. Solenoid valve nonlinear model development

For the modeling of the solenoid valve, a total of 23 different measurements, shown in Figure 10, are used to develop a static model. During this experiment, the pneumatic valve was completely closed and the AC motor was driven at a constant speed by an 8-V input signal.

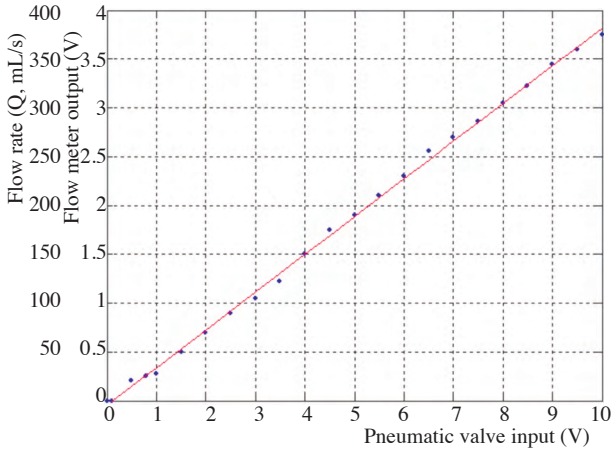

Figure 10. Solenoid valve input-output graph.

The behavior is mostly linear, except for a small region around the origin. The following first-order map:

$$p(x) = 0.38681x - 0.049268, \tag{6}$$

is obtained with optimal L_2 approximation using the input-output pairs shown in Figure 10.

4. Mathematical definition of system performance

In order to assess the performance of a feedback algorithm and to be able to compare 2 different algorithms in a quantitative and objective fashion, precisely defined system performance criteria are needed. To the best of our knowledge, there are no such mathematical performance criteria defined in the literature for similar studies related to physiological blood flow.

To clarify our definition, we would like to stress the fact that the shape of the generated waveform modulo arbitrary time shifts is more important than the shape of the waveform itself. In simpler terms, even if there may be a significant mismatch between the generated flow rate and the desired one, as long as there is a "good" match between a specific delayed version of the generated flow rate and the desired flow rate, one has to consider it as "good" performance in studies of physiological blood flow. As long as one is able to generate a specific waveform very accurately even after some delay, it is possible to reproduce in an in vitro fashion what is happening in an actual blood vessel. Furthermore, transient behavior is not important because one can wait for the system to reach its periodic behavior and then take all of the measurements. More precisely, transient behavior should not be taken into account; what is important is the region after that. One has to consider different delayed versions of the generated waveform and choose the one that results in the best match for the desired flow rate. All of these requirements are captured by the performance definition in Eq. (7). Furthermore, to normalize it, we divide this quantity into the L_1 norm of the input signal over one period. Therefore, we define the system performance as:

$$J = \min_{0 \le \tau \le T} \sum_{t=t_1}^{t_1+T} |x(t) - y(t-\tau)|, \tag{7}$$

where, $x(t)$ is the desired waveform, $y(t)$ is the generated waveform, and the normalized system performance over 100% is defined as:

$$J_n = 100J \Big/ \left(\sum_{t=t_1}^{t_1+T} |x(t)| \right), \tag{8}$$

where T is the period of the waveform and t_1 must be chosen to be much larger than all of the time constants of the closed-loop system, i.e. it must be larger than the duration of transient behavior. Note that we consider the L_1 difference over 1 period between the desired waveform and the generated 1 modulo arbitrary time shift, and we use it as the performance criterion.

In this paper, we consider the coronary artery signal shown in Figure 12 as the reference signal to be tracked, and we compute normalized performance indices J_n for various control algorithms. If the frequency and/or the amplitude of the signal are changed during operation, the performance index is likely to change, and certain algorithms that appear to be superior may turn out to be inferior when this new reference signal is used as a benchmark. Although this is possible, major changes in performance orders are not commonly observed.

5. Use of the PID-based feedback control as a benchmark

In this section, we consider classical PID-based feedback control algorithms and use them as benchmarks for the newly proposed algorithms and their performance analysis. Traditional P, PI, and PID control techniques are among the most widely used basic control techniques. These algorithms first require tuning before actual use, and several algorithms are available for PID tuning. We simply use the Ziegler-Nichols 2 method to obtain the PID coefficients, and we use the resulting controllers and their performances as benchmarks.

As the flow control device, one can use the centrifugal pump, the solenoid valve, or the pneumatic valve. For each alternative, we compute the PID coefficients and then calculate the system performance J_n for the closed-loop flow control system given in Figure 11.

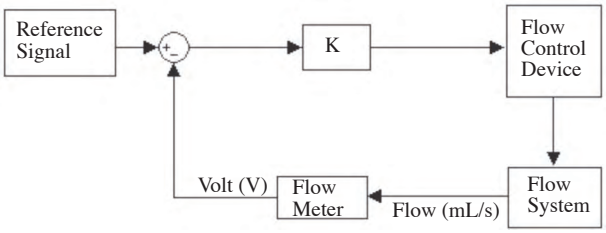

Figure 11. Closed-loop flow control system with the PID controller (K).

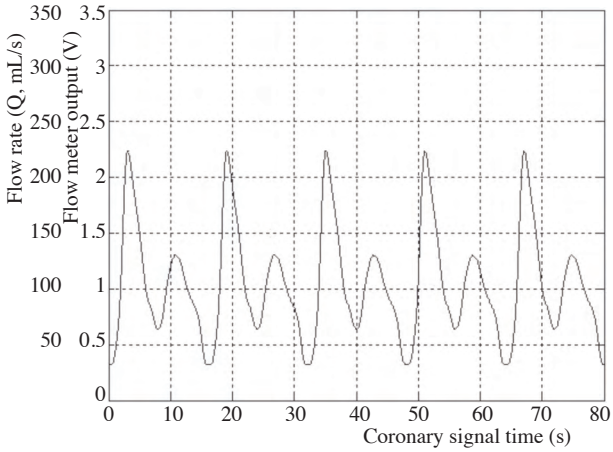

Figure 12. Coronary artery signal used as the reference signal.

The PID coefficients are selected as follows: first, a small proportional gain is selected that will not lead to oscillations in the closed-loop system. The proportional gain, K, is then gradually increased until oscillatory behavior is observed. The corresponding gain and the oscillation period are called the critical gain and the critical oscillation period, and they are denoted by K_o and T_o, respectively. The Ziegler-Nichols 2 method recommends the selection of the PID coefficients given in Table 1.

Table 1. Ziegler-Nichols 2 method for calculation of the initial Kp, Ki, and Kd coefficients.

Type of controller	K_p	K_i	K_d
P	$0.5\ K_o$		
PI	$0.45K_o$	$1.2/T_o$	
PID	$0.6K_o$	$2/T_o$	$T_o/8$

We first operate the closed-loop system shown in Figure 11 with the centrifugal pump acting as the flow control element. The critical gain and oscillation period are determined as $K_o = 0.033$ and $T_o = 1.8421$ s. The same type of experiment is repeated with the pneumatic valve as the flow control element, and then with the solenoid valve. The corresponding critical gain and oscillation periods are determined as $K_o = 0.003$, $T_o = 4.001\ s$ and $K_o = 0.14$, $T_o = 2.12\ s$, respectively.

Throughout this paper, we use the reference signal given in Figure 12 as the test input for all of the performance measurements, which is the coronary artery signal after proper amplitude and time scaling according to the Reynolds and Womersley theory. This signal has a period equal to 16 s for in vitro experimental studies.

The PID coefficients and the associated performance indices for the above mentioned 3 flow control devices are given in Table 2.

Table 2. PID coefficients and the corresponding performance indices for different flow control device alternatives.

Flow control device	Performance indexJ_n	$K_i = 2/T_o = 1.085$ Hz PID coefficients
Centrifugal pump	31.10	$K_p = 0.6\ K_o = 0.0198$ $K_d = T_o/8$=0.2302 s
Pneumatic valve	99.36	$K_i = 2/T_o = 0.5$ Hz $K_p = 0.6\ K_o = 0.0018$ $K_d = T_o/8$=0.5 s
Solenoid valve	23.06	$K_i = 2/T_o = 0.943$ Hz $K_p = 0.6\ K_o = 0.084$ $K_d = T_o/8$=0.2969 s

It is clear that the best system performance under the PID control scheme is obtained when the solenoid valve is used as the flow control device. On the other hand, the pneumatic valve resulted in the worst performance, mainly because of its high hysteresis behavior.

6. Newly proposed control algorithms and performance analysis

In this section, we propose several new closed-loop control algorithms and analyze their performances.

When the centrifugal pump driven by the AC motor and inverter system is used as the flow control device, the pneumatic valve on the main arm is kept at the full open position and the solenoid valve is kept at the full closed position on the parallel pipe. For all other cases, 1 valve is used as the flow control device, the other valve is kept at the full closed position, and the centrifugal pump is driven by an 8-V input signal, which can generate a maximum flow rate of 800 mL/s. The coronary artery flow signal shown in Figure 12 is used as the test input for all of the performance tests.

6.1. P-Σ Control

The P-Σ control system is basically a rate-limited integrator and a proportional gain, as shown in Figure 13. It has been observed that the rate limiter improves the overall system performance. It can be applied to all of the 3 flow control devices: the centrifugal pump, the pneumatic valve, and the solenoid valve. The main idea behind P-Σ control is to make only incremental changes relative to the current position of the valve or the current speed of the motor, and to impose a rate limit to avoid unwanted oscillations. If $c(t)$ is the command sent to the flow control device, $r(t)$ is the desired flow rate, and $m(t)$ is the measured flow rate, the P-Σ controller can be described by:

$$c(t) = rLim(K_p(r(t) - m(t)) + c(t-1)), \tag{9}$$

where $rLim$ is the rate limiter function.

6.1.1. P-Σ control with the centrifugal pump

When we use the K_p value obtained from the Zeigler-Nichols 2 method, with the absolute value of the derivative of the input bounded by 5, about 51% improvement (reduction) is observed on performance index J_n (see Table 3). The closed-loop system behavior is given in Figure 14. We would like to emphasize that this performance is even better than the PID control with the solenoid valve, which was the best performance obtained for the PID control.

Table 3. P-Σ control error performance with the centrifugal pump.

K_p	Performance index J_n
0.0165	15.11

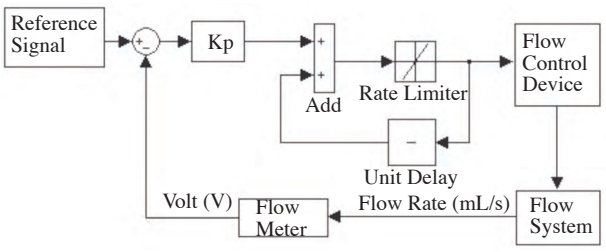

Figure 13. P-Σ controller.

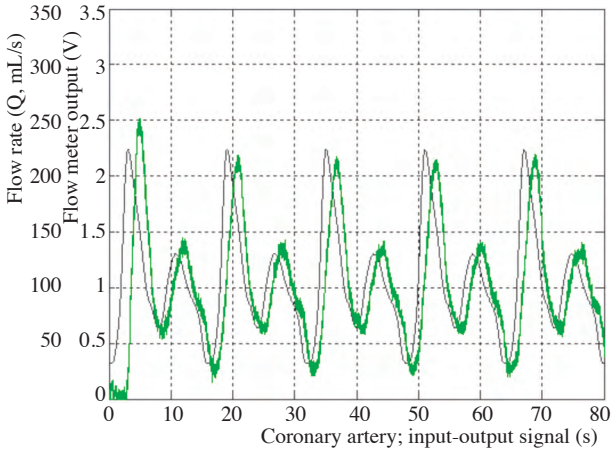

Figure 14. Closed-loop system behavior for P-Σ control with the centrifugal pump.

6.1.2. P-Σ control with the pneumatic valve

In this experiment, we use the K_p value obtained from the Zeigler-Nichols 2 method, with the absolute value of the derivative of the input bounded by 5, and about 69% improvement (reduction) is observed on performance

index J_n (see Table 4). The closed-loop system behavior is given in Figure 15. The resulting performance is close to the performance obtained from the centrifugal pump driven by the AC motor + inverter system. Although the pneumatic valve has high hysteresis behavior, and hence is more difficult to control, by using an improved control algorithm, we were able to achieve the PID performance of a less problematic device, i.e. the centrifugal pump.

Table 4. P-Σ control error performance with the pneumatic valve.

K_p	Performance index J_n
0.0015	31.01

6.1.3. P-Σ control with the solenoid valve

The solenoid valve had the best PID performance for the benchmark tests given in Section 5. We observe a similar trend here for the P-Σ control. When we use the K_p value obtained from the Zeigler-Nichols 2 method, with the absolute value of the derivative of the input bounded by 5, about 66% improvement (reduction) is observed on performance index J_n (see Table 5). The closed-loop system behavior is given in Figure 16.

Table 5. P-Σ control error performance with the solenoid valve.

K_p	Performance index J_n
0.03	7.78

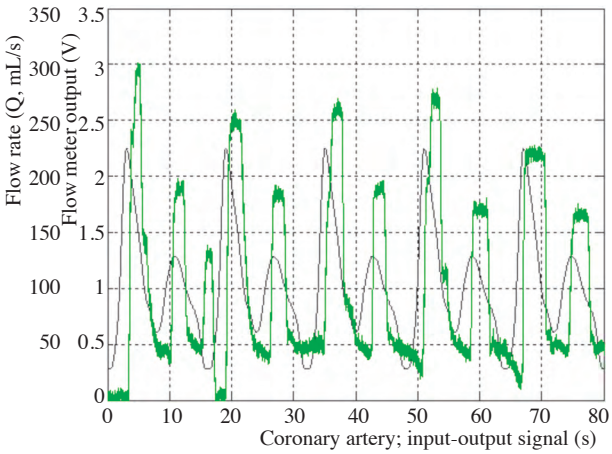

Figure 15. Closed-loop system behavior for P-Σ control with the pneumatic valve.

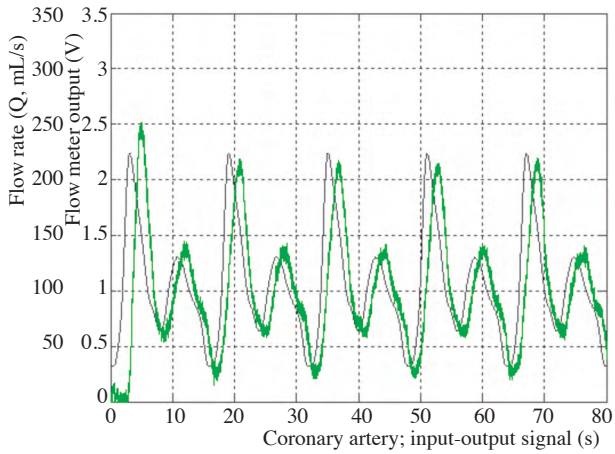

Figure 16. Closed-loop system behavior for P-Σ control with the solenoid valve.

It is clear from the PID performance experiments and P-Σ control performance tests that the pneumatic valve has the worst performance among the 3 competing flow control technologies. This is mainly because of its highly nonlinear behavior, hysteresis characteristics, and slow response. Therefore, in the rest of the paper, we only consider the centrifugal pump and the solenoid valve as flow control devices, and we test the newly proposed control algorithms only on these 2 devices.

6.2. P-Σ predictive control

The P-Σ control system is basically a rate-limited integrator and a proportional gain, as shown in Figure 13. However, its main logic is simply based on reducing the steady-state error, and there is no built in mechanism to improve the dynamic "performance". The P-Σ predictive control has an extra prediction subblock, as shown in Figure 17, which introduces an additional control action. This additional control action is to open the valve a little bit more, or to increase the centrifugal pump speed a little bit more, whenever an increasing trend is observed in the desired flow rate. This prediction subblock has a similar but opposite effect for a decreasing trend in the desired flow rate.

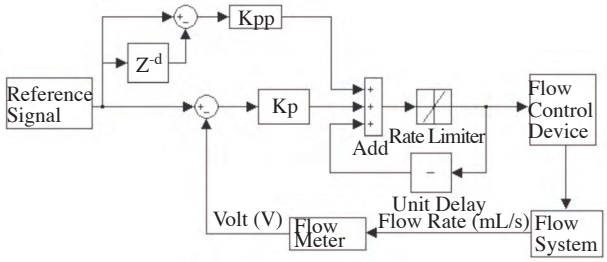

Figure 17. P-Σ predictive controller.

The controller equation is given as:

$$c(t) = rLim(K_{pp}(r(t) - r(t-d)) + K_p(r(t) - m(t)) + c(t-1)), \tag{10}$$

where the $K_{pp}(r(t) - r(t-d))$ term takes the difference between the current and past desired flow rates. Based on the assumption that the observed trend will continue in the same way in the near future, this term is expected to adjust the control effort in a more effective fashion before it is too late, and a bigger error is observed between the measured and desired flow rates.

6.2.1. P-Σ predictive control with the centrifugal pump

In a P-Σ predictive controller, there are 2 parameters to be determined, K_{pp} and d. We first fix the delay d to 75 samples and try to find a reasonable prediction coefficient K_{pp}. We then change the delay d and search for the best possible performance index J_n (see Table 6).

Table 6. P-Σ predictive control error performance with the centrifugal pump.

Delay d	K_{pp}	K_p	Performance index J_n
75	0.001	0.01	17.1757
75	5e-5	0.01	15.7453
25	5e-5	0.01	16.1856
150	**5e-5**	**0.01**	**15.2952**

Although different prediction coefficients and delay terms resulted in different closed-loop performance indices, no major improvement was observed by adding the predictive action to the P-Σ controller with the centrifugal pump. Although it is not always the case, adding a predictive action is expected to improve the performance, and one reason why we do not observe a major improvement here is the possibility of a built-in prediction mechanism in the centrifugal pump driver, which is a professional industrial grade microprocessor

controlled by a complex power electronics system. Other probable reasons are measurement/experimental errors or an insufficient search in the $K_{pp} - d$ plane.

6.2.2. P-Σ predictive control with the solenoid valve

The P-Σ predictive controller results in a significant improvement compared to the P-Σ controller when the solenoid valve is used as the flow control device. More precisely, we were able to improve performance index J_n by 29% by searching for a suitable prediction coefficient and a delay value in the $K_{pp} - d$ plane (see Table 7).

Table 7. P-Σ predictive control performance with the solenoid valve.

Delay d	K_{pp}	K_p	Performance index J_n
75	0.001	0.03	5.6578
100	**0.001**	**0.03**	**5.5378**
125	0.001	0.03	5.9306

6.3. P-Σ look-ahead control

The P-Σ look-ahead controller is basically the P-Σ controller with the look-ahead feature. Indeed, it can be classified as a different predictive P-Σ controller, but the prediction of the trend is based on future samples, not the past values. Mathematically, the P-Σ look-ahead controller is given by:

$$c(t) = rLim(K_{pp}(r(t+d) - r(t)) + K_p(r(t) - m(t)) + c(t-1)). \tag{11}$$

However, due to the noncausal nature of the controller, its HIL implementation is done as described in Figure 18, which can be expressed by the causal control equation:

$$c(t) = rLim(K_{pp}(r_1(t) - r_1(t-d)) + K_p(r_1(t-d) - m(t)) + c(t-1)), \tag{12}$$

where $r_1(t) = r(t+d)$. Since the performance index is not affected by overall time-shifts,

$$J = \min_{0\le\tau\le T} \sum_{t=t_1}^{t_1+T} (r(t) - m(t-\tau))^2 = \min_{0\le\tau\le T} \sum_{t=t_1}^{t_1+T} (r_1(t) - m(t-\tau))^2, \tag{13}$$

the performance of the original noncausal P-Σ look-ahead controller can be computed by using the system given in Figure 18.

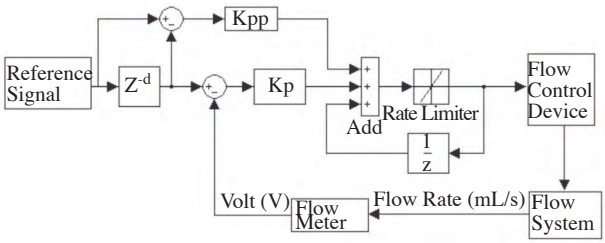

Figure 18. P-Σ look-ahead controller.

6.3.1. P-Σ look-ahead control with centrifugal pump

The P-Σ look-ahead controller results in an improvement compared to the PID and P-Σ controller when the centrifugal pump is used as the flow control device. We were able to improve the performance index J_n up to 12% by searching for a suitable prediction coefficient and a delay value in the $K_{pp} - d$ plane (see Table 8).

Table 8. P-Σ look-ahead controller performance with the centrifugal pump.

Delay d	K_{pp}	K_p	Performance index J_n
75	0.0075	0.0165	15.7784
100	**0.0075**	**0.0165**	**13.2685**
125	0.0075	0.0165	13.6301

6.3.2. P-Σ look-ahead control with the solenoid valve

Similar to the performance improvements observed for the centrifugal pump, the look-ahead technique also resulted in an improvement. Compared to the P-Σ controller, the look-ahead technique resulted in 20% performance improvement, which is comparable to the performance improvement observed with causal prediction. The search results for a suitable prediction coefficient and a delay value in the $K_{pp} - d$ plane are summarized in Table 9.

Table 9. P-Σ look-ahead controller performance with solenoid valve.

Delay d	K_{pp}	K_p	Performance index J_n
50	0.01	0.03	6.2608
75	**0.01**	**0.03**	**6.2531**
100	0.01	0.03	6.2767

The results of subsections 6.1, 6.2, and 6.3 can be summarized as follows: the use of the P-Σ technique did improve the performance compared to that of the Ziegler-Nichols 2 PID. Furthermore, prediction techniques, either in the form of causal or noncausal, did further improve the performance compared to the simple "predictionless" P-Σ controller.

In the following 3 subsections, we analyze the feed-forward control, which is based on an inversion of the model developed in Section 3, and then consider the effects of causal and noncausal prediction.

6.4. Feed-forward control

In Section 3, static models of each flow control device were developed based on the experimental data. Flow control devices are not simple static nonlinearities, and they also do have dynamic behavior. Nevertheless, these static models are still an approximate representation, and the inverse of these static models can be used as an approximation of the inverse of the flow control device. The resulting error due to approximation errors can be compensated by proportional control techniques. The authors were able to find similar work in [27]; however, most of the details were very sketchy. We propose 2 different feed-forward controller architectures, as shown in Figures 19 and 20.

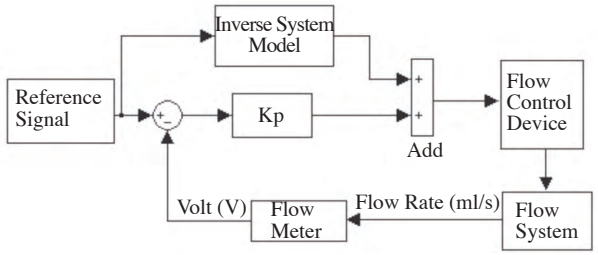

Figure 19. Type-1 feed-forward control.

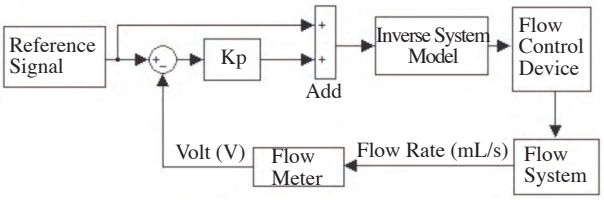

Figure 20. Type-2 feed-forward control.

The type-1 feed-forward controller can be described by the following equation:

$$c(t) = K_p(r(t) - m(t)) + g(r(t)), \tag{14}$$

whereas the type-2 feed-forward controller equation is:

$$c(t) = g\left(K_p(r(t) - m(t)) + r(t)\right), \tag{15}$$

where g is the inverse of the static nonlinear model of the flow control device. The inverse function g can be computed using inverted polynomial interpolation. In MATLAB-based experiments, we used a table look-up block for inverse function realization.

In the following subsections, both types of feed-forward controllers are analyzed from a performance point of view.

6.4.1. Feed-forward control with centrifugal pump

In order to tune the feed-forward controller, a one-dimensional search in the K_p space is necessary. Controller tuning results are summarized in Tables 10 and 11 for type-1 and type-2 feed-forward controllers, respectively. Compared to the best possible performance index of 13.2685 among the PID, P-Σ, P-Σ predictive, and P-Σ look-ahead controllers with a centrifugal pump, a major performance improvement of 42% was achieved.

Table 10. Type-1 feed-forward controller performance with the centrifugal pump.

K_p	Performance index J_n
0.01	14.7968
0.75	**7.6778**
1	8.9580

Table 11. Type-2 feed-forward controller performance with the centrifugal pump.

K_p	Performance index J_n
0.5	9.6623
0.75	**8.7538**
1	10.8726

6.4.2. Feed-forward control with solenoid valve

For the solenoid valve, we conducted a similar one-dimensional search in the K_p space, and the results are summarized in Tables 12 and 13 for type-1 and type-2 feed-forward controllers, respectively. Compared to the best possible performance index of 5.5378 among the PID, P-Σ, P-Σ predictive, and P-Σ look-ahead controllers with a solenoid valve, a small performance improvement of about 3% was achieved.

Table 12. Type-1 feed-forward controller performance with the solenoid valve.

K_p	Performance index J_n
0.1	10.5214
0.75	**6.6234**
1	6.8689

Table 13. Type-2 feed-forward controller performance with the solenoid valve.

K_p	Performance index J_n
0.5	5.5849
0.75	**5.3783**
1	5.4590

6.5. Feed-forward predictive and look-ahead controllers

In the previous subsections, we demonstrated that the prediction block did improve the performance for the P-Σ family of controllers (see Figure 21). We will also use the same technique here for possible further improvements.

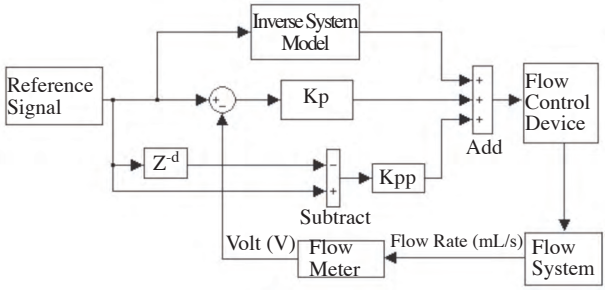

Figure 21. Feed-forward predictive controller.

The controller equation is:

$$c(t) = g(r(t)) + K_p(r(t) - m(t)) + K_{pp}\left(r(t) - r(t-d)\right), \tag{16}$$

where K_p is the proportional gain, K_{pp} is the prediction coefficient, and d is the delay. Tuning this controller requires a 3-dimensional search in the $K_p - K_{pp} - d$ space. Tuning results for the control with the centrifugal pump and solenoid valve are given in Tables 14 and 15, respectively.

Table 14. Feed-forward predictive controller performance with the centrifugal pump.

Delay d	K_{pp}	K_p	Performance index J_n
75	0.75	0.01	8.2903
75	**0.75**	**1e-5**	**7.4599**
75	0.75	1e-6	8.3885

Table 15. Feed-forward predictive controller performance with the solenoid valve.

Delay d	K_{pp}	K_p	Performance index J_n
50	0.75	0.6	6.4887
100	**0.75**	**0.6**	**5.2319**
150	0.75	0.6	5.5466

In both cases, about 3% improvement is observed in system performance compared to the "predictionless" feed-forward control. As with the P-Σ controllers, we also tested the look-ahead techniques as a noncausal alternative "trend prediction" technique. However, no further improvement was observed. This is mostly likely because we reached certain performance limits, either because of the nature of the control techniques used or the intrinsic characteristics of the flow system (plant).

7. Results and discussion

In this paper, we studied pulsatile flow generation using newly proposed closed-loop control algorithms for in vitro blood flow research. Throughout the paper, a coronary artery flow signal was used; however, the techniques developed in this paper can be applied for blood flow signals measured from other parts of the human body, as well. In the literature, there are several published research papers using open-loop control, and the performance assessment was mostly graphical. To the best of the authors' knowledge, there has been no extensive study on the use of closed-loop control techniques for pulsatile flow generation for in vitro blood flow research. There are 3 main achievements in this paper: 1) both model-based and heuristic closed-loop control techniques are developed; 2) a meaningful mathematical performance objective, which is also suitable and consistent with the nature of the problem, is defined; and 3) all of the performance analyses and comparative evaluation studies are based on this mathematical performance index. With the centrifugal pump used as the flow control device, about 7% error is observed in synthesizing the coronary artery flow signal, and with the solenoid valve, about 5% error. This is about 75% improvement compared to the classical Ziegler-Nichols 2 PID controller. A closer examination of Figures 22 and 23 demonstrates the effectiveness of the proposed techniques.

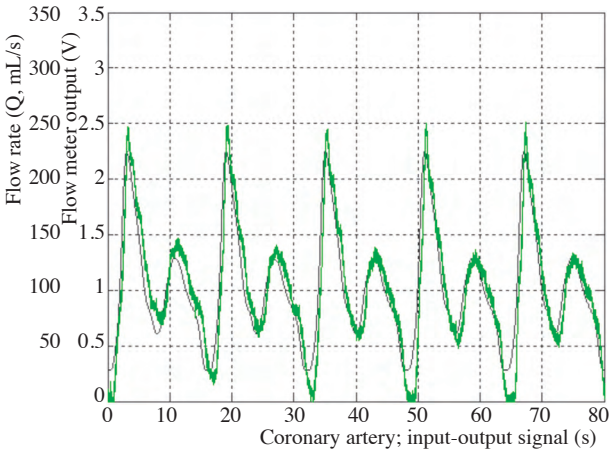

Figure 22. Best performance for the centrifugal pump is obtained with the feed-forward predictive control when the reference signal is the coronary artery blood flow signal. The performance is computed as $J = 7.4599$.

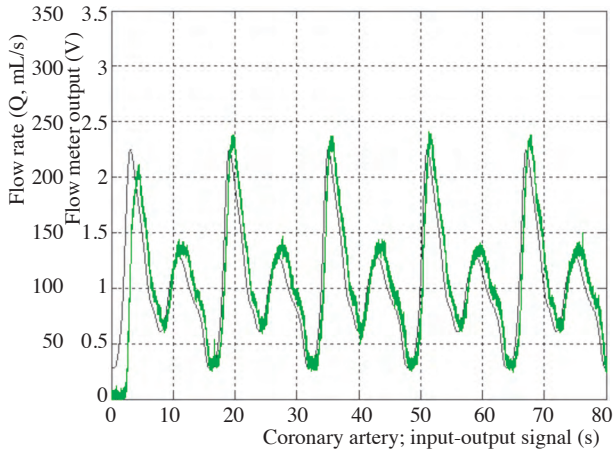

Figure 23. Best performance for the solenoid valve is obtained with the feed-forward predictive control when the reference signal is the coronary artery blood flow signal. The performance is computed as $J = 5.2319$.

More detailed findings of the paper can be summarized as follows:

1. The pneumatic valve had the worst performance among the 3 competing flow control technologies, mainly because of its highly nonlinear behavior, hysteresis characteristics, and slow response. The solenoid valve had the best performance for most of the cases, and the centrifugal pump had slightly worse performance

compared to that of the solenoid valve.

2. Among the newly proposed control techniques, the P-Σ controller resulted in 51%-69% better performance compared to the PID. When either causal or noncausal prediction was added to the controller, it usually resulted in performance improvements. The P-Σ predictive controller, which is basically a causal predictive controller, resulted in 29% performance improvement compared to the P-Σ controller when the solenoid valve was used as the flow control device. However, causal prediction did not result in a significant performance improvement when the centrifugal pump was used as the flow control device. The P-Σ look-ahead controller, which is a noncausal predictive controller, resulted in 12%-20% improvement compared to the predictionless P-Σ controllers for both the solenoid valve and the centrifugal pump. The performance improvement was more significant for the solenoid valve. In summary, the use of the P-Σ technique did improve performance compared to that of the Ziegler-Nichols 2 PID. Furthermore, prediction techniques, either in the form of causal or noncausal, did further improve performance compared to the simple "predictionless" P-Σ controller.

3. The feed-forward controllers did result in further performance improvements. Predictionless feed-forward controllers based on static nonlinear models resulted in up to 42% performance improvement compared to the PID, P-Σ, P-Σ predictive, and P-Σ look-ahead controllers. The addition of prediction did further improve performance by about 3%.

4. Among the newly proposed techniques, predictive feed-forward controllers based on static nonlinear models resulted in the best performance.

For future research, we plan to consider dynamic models instead of static models, robust control-oriented modeling, incorporation of time-varying "unmodeled dynamics" blocks, and the use of more advanced control theory and techniques to further improve these results.

References

[1] D. Liepsch, "An introduction to biofluid mechanics basic models and applications", Journal of Biomechanics, Vol. 35, pp. 415-435, 2002.

[2] D.N. Ku, "Blood flow in arteries", Annual Review of Fluid Mechanics, Vol. 29, pp. 399-434, 1997.

[3] R.M. Berne, M.N. Levy, Cardiovascular Physiology, St. Louis, Mosby, 1986.

[4] A. Kamiya, T. Togawa, "Adaptive regulation of wall shear stress to flow change in the canine carotid artery", American Journal of Physiology - Heart and Circulatory Physiology, Vol. 293, pp. 14-21, 1980.

[5] S.W. Galt, R.M. Zwolak, R.J. Wagner, J.J. Gilbertson, "Differential response of arteries and vein grafts to blood flow reduction", Journal of Vascular Surgery, Vol. 17, pp. 563-570, 1993.

[6] S.Q. Liu, Y.C. Fung, "Relationship between hypertension, hypertrophy, and opening angle of zero-stress state of arteries following aortic constriction", Journal of Biomechanical Engineering, Vol. 111, pp. 325-333, 1989.

[7] J.I. Hoffman, S. Kaplan, "The incidence of congenital heart disease", Journal of the American College of Cardiology. Vol. 39, pp. 1890-900, 2002.

[8] C.A. Taylor, M.T. Draney, "Experimental and computational methods in cardiovascular fluid mechanics", Annual Review of Fluid Mechanics, Vol. 231, pp. 36-197, 2004.

[9] F. Loth, P.F. Fischer, N. Arslan, C.D. Bertram, S.E. Lee, T.J. Royston, W.E. Shaalan, H.S. Bassiouny, "Transitional flow at the venous anastomosis of an arteriovenous graft: potential activation of ERK1/2 mechanotransduction pathway", Journal of Biomechanical Engineering, Vol. 125, pp. 49-61, 2003.

[10] T.M. Liou, Y.C. Li, "Effects of stent porosity on hemodynamics in a sidewall aneurysm model", Journal of Biomechanics, Vol. 41, pp. 1174-1183, 2008.

[11] N. Arslan, F. Loth, C.D. Bertram, H.S. Bassiouny, "Transitional flow field characterization inside an arteriovenous graft-to-vein anastomosis under pulsatile flow conditions", European Journal of Mechanics - B/Fluids, Vol. 24, pp. 353-365, 2005.

[12] S.W. Lee, D.S. Smith, F. Loth, P.F. Fischer, H.S. Bassiouny, "Numerical and experimental simulation of transitional flow in a blood vessel junction", Numerical Heat Transfer, Part A: Applications, Vol. 51, pp. 1-22, 2007.

[13] J. Peacock, T. Jones, C. Tock, R. Lutz, "An in vitro study on the effect of branch points on the stability of coronary artery flow", Medical Engineering & Physics, Vol. 19, pp. 101-108, 1997.

[14] S.C.M. Yu, "Steady and pulsatile flow studies in abdominal aortic aneurysm models using particle image velocimetry", International Journal of Heat and Fluid Flow, Vol. 21, pp. 74-83, 2000.

[15] S. Sivenesan, T.V. How, R.A. Black, A. Bakran, "Flow pattern in the radiocephalic arteriovenous fistula: an in vitro study", Journal of Biomechanics, Vol. 32, pp. 915-925, 1999.

[16] H.M. Crawshaw, W.C. Quist, E. Serallach, C.R. Valeri, F.W. LoGerfo, "Flow disturbance at the distal end-to-side anastomosis - effect of patency of the proximal outflow segment and angle of anastomosis", Archives of Surgery, Vol. 115, pp. 1280-1284, 1980.

[17] M. Nakamura, W. Sugiyama, M. Haruna, "An experiment on the pulsatile flow at transitional Reynolds numbers – the fluid dynamical meaning of the blood-flow parameters in the aorta", Journal of Biomechanical Engineering, Vol. 115, pp. 412-417, 1993.

[18] R.A. Peattie, "Experimental study of pulsatile flow in models of abdominal aortic aneurysms", IEEE Engineering in Medicine and Biology Society, Vol. 20, pp. 367-370, 1998.

[19] N. Arslan, "An in vitro investigation of steady transitional flow in an arteriovenous graft-to-vein anastomosis", Turkish Journal of Engineering & Environmental Sciences, Vol. 37, pp. 79-81, 2007.

[20] T.M. Liou, Y.C. Li, "Effects of stent porosity on hemodynamics in a sidewall aneurysm model", Journal of Biomechanics, Vol. 41, pp. 1174-1183, 2008.

[21] N. Arslan, A.B. Sengul, "Experimental detection of critical flow regions inside a complex graft to vein connection using laser Doppler anemometer", Experimental Techniques, Vol. 34, pp. 30-37, 2009.

[22] C.D. Bertman, F. Pythoud, N. Stergiopulos, J.J. Meister, "Pulse wave attenuation measurement by linear and nonlinear methods in nonlinearly elastic tubes", Medical Engineering and Physics, Vol. 21, pp. 155-166, 1999.

[23] G. Pennati, G.B. Fiore, F. Migliavacca, K. Laganà, R. Fumero, G. Dubini, "In vitro steady-flow analysis of systemic-to-pulmonary shunt haemodynamics", Journal of Biomechanics, Vol. 34, pp. 23-30, 2001.

[24] I. Van Tricht, D. De Wachter, J. Tordoir, P. Verdonck, "Hemodynamics in a compliant hydraulic in vitro model of straight versus tapered PTFE arteriovenous graft", Journal of Surgical Research, Vol. 116, pp. 297-304, 2004.

[25] A. Schmidt, T. da Silva Júnior, A. Pazin-Filho, L. Otávio Murta Júnior, O. César Almeida-Filho, L. Gallo-Júnior, J. Antonio Marin-Neto, B. Carlos Maciel, "Effects of changing blood viscosity and heart rate on vena contracta width as evaluated by color Doppler flow mapping. An in vitro study with a pulsatile flow model", Echocardiography, Vol. 25, pp. 133-140, 2008.

[26] W. Tsai, Ö. Savaş, "Flow pumping system for physiological waveforms", Medical & Biological Engineering & Computing, Vol. 48, pp. 197-201, 2010.

[27] J.D. Bomberger, D.E. Seborg, "Determination of model order for NARX models directly from input-output data", Journal of Process Control, Vol. 8, pp. 459-468, 1998.